



# Phase transition of nickel silicide compounds and their electrical properties

Razvan Pascu<sup>1,2,3,\*</sup>  and Cosmin Romanitan<sup>1</sup>

<sup>1</sup>National Institute for Research and Development in Microtechnologies – IMT Bucharest, Bucharest, Romania

<sup>2</sup>University “Politehnica” of Bucharest, Bucharest, Romania

<sup>3</sup>Romanian Young Academy – Research Institute of the University of Bucharest, Bucharest, Romania

**Received:** 11 February 2021

**Accepted:** 20 May 2021

**Published online:**  
28 May 2021

© The Author(s), under exclusive licence to Springer Science+Business Media, LLC, part of Springer Nature 2021

## ABSTRACT

An experimental study concerning the effects of post-metallization annealing treatments in inert atmosphere on the metal/semiconductor junction has been assessed. Thus, both Schottky and ohmic contacts on n-type Si substrates using Ni and nickel silicide as gate electrode have been fabricated and a correlation between their microstructure changes and the electrical parameters has been realised. The X-ray diffraction measurements showed the presence of Ni<sub>2</sub>Si and NiSi crystalline phases at low temperature annealing, which are then converted to NiSi<sub>2</sub> and NiSi when high temperatures are used. In addition, the mean crystallite size and dislocation density have been estimated and significant improvements were achieved for the annealed samples. The role of Ni/Si interfaces was further demonstrated by electrical investigation of the fabricated structures. A significant diminishing of the contact resistance, transfer length and specific contact resistivity has been confirmed. In the case of the Schottky diodes, an increase in the current with almost two order of magnitude after a post-metallization annealing at a temperature of 900 °C has been obtained.

## 1 Introduction

The Schottky diode (SD) represents the most frequently used electronic device in a wide range of applications. Owing to the low forward voltage drop and fast response, SD can be a successful candidate for high-speed logic circuits, solar cells or different types of sensors (temperature, gas, optical). Moreover, albeit studies regarding the metal/semiconductor (MS) contacts have been regularly reported in the last four decades, fabrication of a very

stable contact remains an unsolved issue, even if it is designed to work as rectifying element (Schottky diode) or as an ohmic one. The physical properties of the MS interface are strongly influenced by the preparation conditions, principally the metal deposition method and the different post-metallization annealing (PMA) treatments performed [1]. In this context, the metal silicide compound was primarily investigated due to the low resistivity of the metal/semiconductor contact [2, 3]. A high-quality silicide compounds are characterised by low Si consumption,

Address correspondence to E-mail: razvan.pascu@imt.ro

low resistivity, as low as possible processing temperatures and high temperature operational stability. NiSi meets successfully all these criteria, having the lowest resistivity, as well as chemical and thermal stabilities. Consequently, it plays an important role in modern electronic devices technology [4, 5]. However, in the Ni–Si phase diagram, three dominant phases, namely Ni<sub>2</sub>Si, NiSi and NiSi<sub>2</sub>, could be present, depending on the annealing temperature [6]. Since they lead to different values for film resistivity, their accurate identification becomes crucial to appreciate the electrical performances of the contacts. Microstructural and compositional investigations, such as electron energy-loss spectroscopy [7, 8] and energy-dispersive X-ray spectroscopy in correlation with scanning transmission electron microscopy [9, 10] are generally used to determine both the resultant phases and the chemical bonding.

Furthermore, a high-quality Schottky diode is characterised by two essential parameters: the Schottky Barrier Height (SBH) and the ideality factor ( $n$ ). The electrical performances are significantly improved if the ohmic contact used as the back contact for SDs assures a low series resistance to reduce the losses during the operation. However, the SBH is the main parameter for detection when the SD acts as sensor. The experimental value of the SBH in the case of a NiSi or NiSi<sub>2</sub>/n-type Si system is around 0.65 eV [11], but it can be varied by different methods, such as sulphur segregation during Ni silicidation [12] or performing post-metallization annealing treatments in inert atmosphere [13]. A critical issue in the MS contacts' fabrication is the occurrence of small 'patches' with different SBHs on the designed active area [14, 15]. They are caused by the mixture of different phases resulted during a PMA treatment, seriously affecting the current across the MS contact. Thus, the inhomogeneous contact formed leads to voltage-dependent SBH [16, 17], destroying the device stability.

Consequently, finding the most appropriate fabrication technology to obtain finally very stable barriers with high contact homogeneity and smooth MS interface represents a challenge. The goal of this study is to develop and optimise the MS contacts for different sensing applications, for instance temperature [18, 19] or gas [20] sensors. Our previous results demonstrated the necessity of a PMA treatment in Ar atmosphere in the case of a Ni/SiC Schottky diode fabricated for high-temperature sensor application [21, 22]. Significant improvements concerning both

the Ni crystallinity and the Schottky diode electrical characteristics were reported. Regarding the Ni/Si heterojunction, we firstly investigated the microstructure and composition resulted after different PMA treatments [23].

Herein we report a systematic analysis, where the electrical characterisation of different MS contacts (ohmic contacts, vertical and back-to-back Schottky diodes) was completed by rigorous microstructural investigation based on the X-ray diffraction analysis. Our primary interest in this work was to find the appropriate experimental technology for fabrication of reliable MS contacts. We have studied and clarified the mechanisms involved in the modification of the electrical parameters as function of the post-metallization annealing treatments, looking at microstructure changes induced at interface. We demonstrated that the microstructural parameters, such as phase changes, crystallite size and dislocation density, directly influence the electrical performances of the fabricated samples and we indicated in what way they act. Thus, we showed that high values for crystallite size and low dislocation density are found when a phase reach in Si (NiSi<sub>2</sub>), obtained for high temperature annealing, is present. They led to better rectifying performances and improved electrical parameters for the Schottky diodes.

## 2 Experimental details

The test samples have been fabricated starting from n-type Si (100) wafers with 5–10  $\Omega$  cm resistivity, purchased from Siegert Wafer GmbH. Initially, all the wafers were degreased in acetone and methanol (5 min), then soaked in "Piranha" solution (H<sub>2</sub>SO<sub>4</sub>:H<sub>2</sub>O<sub>2</sub>—3:1 v/v) at 130 °C for 15 min and rinsed in deionised water (DIW). After this procedure, the resulted thin film of oxide was removed by immersing the wafers in 5% (v/v) aqueous HF for 5 min, rinsed with deionised water and dried under N<sub>2</sub>.

Next, the fabrication process flow was adapted to realise the three different types of structures designed: *ohmic contacts*, *vertical Schottky diodes* where the best performing ohmic contact was used as backside contact and *back-to-back Schottky diodes* with identical designed areas and different rapid PMA treatments both at low and high temperature.

### 2.1 Ohmic contact fabrication

First, a phosphorous diffusion process was performed in  $\text{POCl}_3$  atmosphere at  $950\text{ }^\circ\text{C}$  for 30 min to obtain a heavily doped Si layer on the wafer backside. To define the active areas for Transfer Length Method (TLM) measurements,  $500\text{ nm}$   $\text{SiO}_2$  film has been deposited by Low Pressure Chemical Vapour Deposition (LPCVD) technique on the heavily doped side of the Si wafer (backside). Using standard photolithographic processes, we have opened windows in the deposited oxide, defining the active pads of the final structures. Next, a Ni thin film ( $100\text{ nm}$ ) was deposited by sputtering and patterned using a second photolithographic process (wet etching of the metal). The main steps of the fabrication process flow and the designed final structure are presented in Fig. 1a and b, respectively.

The as-deposited Ni ohmic contacts (called AD) have been evaluated in comparison with the ones subjected to a rapid PMA in Ar atmosphere, at a temperature of  $1050\text{ }^\circ\text{C}$  for 3 min (called 1050). The structures were packaged in DIL 40 capsules using the wire bonding technology, as it is shown in Fig. 1c. The main parameters, such as: the sheet resistance ( $R_{sh}$ ), the contact resistance ( $R_c$ ), the transfer length ( $L_T$ ) and the specific contact resistivity ( $\rho_c$ ) have been determined from the electrical measurements' data.

The ohmic contacts are characterised by the specific contact resistivity that can be estimated using the

Transfer Length Method [24]. Consequently, an array of contact pads with the width of  $150\text{ }\mu\text{m}$  ( $W$ ), separated by successively increased distances between them ( $10, 20, 30, 40$  and  $50\text{ }\mu\text{m}$ ), have been designed and fabricated, as it is shown in Fig. 1b.

### 2.2 Vertical and back-to-back Schottky diodes fabrication

Next, the technology established for best performances ohmic contact ( $1050\text{ }^\circ\text{C}$  PMA, 3 min, Ar atmosphere) has been used to complete the fabrication process flow of both vertical and back-to-back Schottky diodes (i.e. Si wafer frontside—Schottky structures; Si wafer backside—ohmic contact). The technological flow is presented in the diagram from Fig. 2a.

Two identical circular areas ( $400\text{ }\mu\text{m}$ —diameter) for Schottky diodes have been designed, as can be seen in Fig. 2b, in order to test both vertical and back-to-back Schottky diodes. To define the active areas of the Schottky contacts,  $500\text{ nm}$   $\text{SiO}_2$  film was deposited using LPCVD technique. In this field oxide, two circular windows have been opened using standard photolithographic processes. The Schottky metal ( $100\text{ nm}$  Ni) was defined in these opened windows. Subsequently, different PMA treatments in Ar atmosphere, at both low (i.e.  $350$  and  $400\text{ }^\circ\text{C}$ ) and high temperatures (i.e.  $850$  and  $900\text{ }^\circ\text{C}$ ), were performed for 3 min to study their influence of the

**Fig. 1** **a** Diagram for the experimental procedure—technological flow of the ohmic contacts; **b** 3D view of the designed ohmic contact structures; **c** the photograph of the fabricated structures encapsulated in a DIL 40 package using wire bonding technology

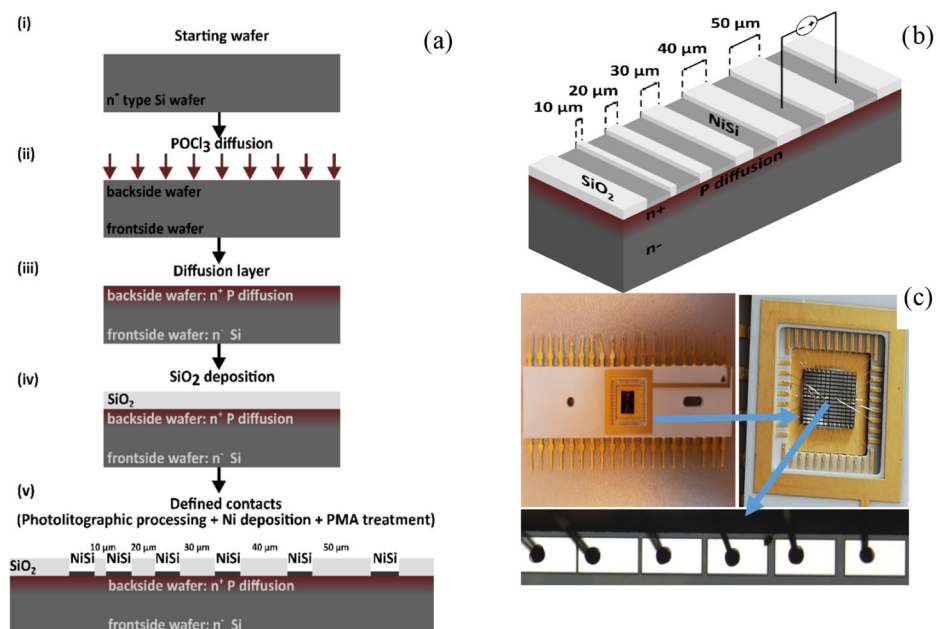
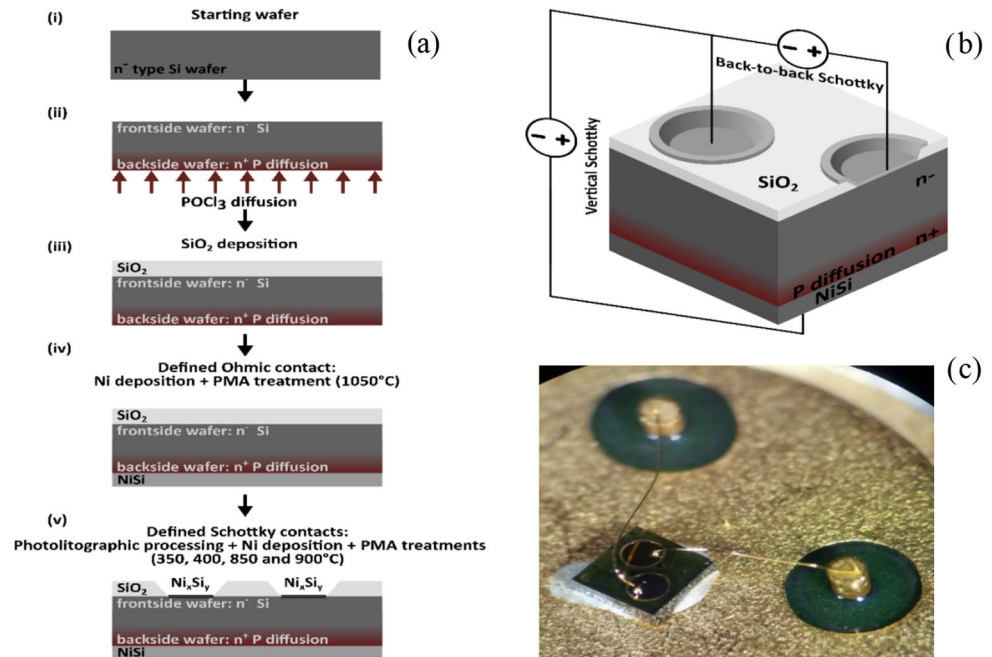


**Fig. 2** a Diagram for the experimental procedure—technological flow of the Schottky diodes; b 3D view of the designed Schottky diodes; c the photograph of the fabricated structures encapsulated in a TO-39 package using wire bonding technology



microstructural and electrical properties of the Schottky diodes. The final structures have been encapsulated in compact TO-39 packages using wire bonding technology (Fig. 2c).

In order to evaluate the electrical performances of the fabricated samples, the main electrical parameters were determined using standard current–voltage (*I*–*V*) characteristics: Schottky Barrier Height—SBH ( $\Phi_{Bn}$ ), ideality factor (*n*), saturation current (*I<sub>s</sub>*) and series resistance (*R<sub>s</sub>*).

### 3 Results and discussions

#### 3.1 Microstructural investigations using XRD analysis

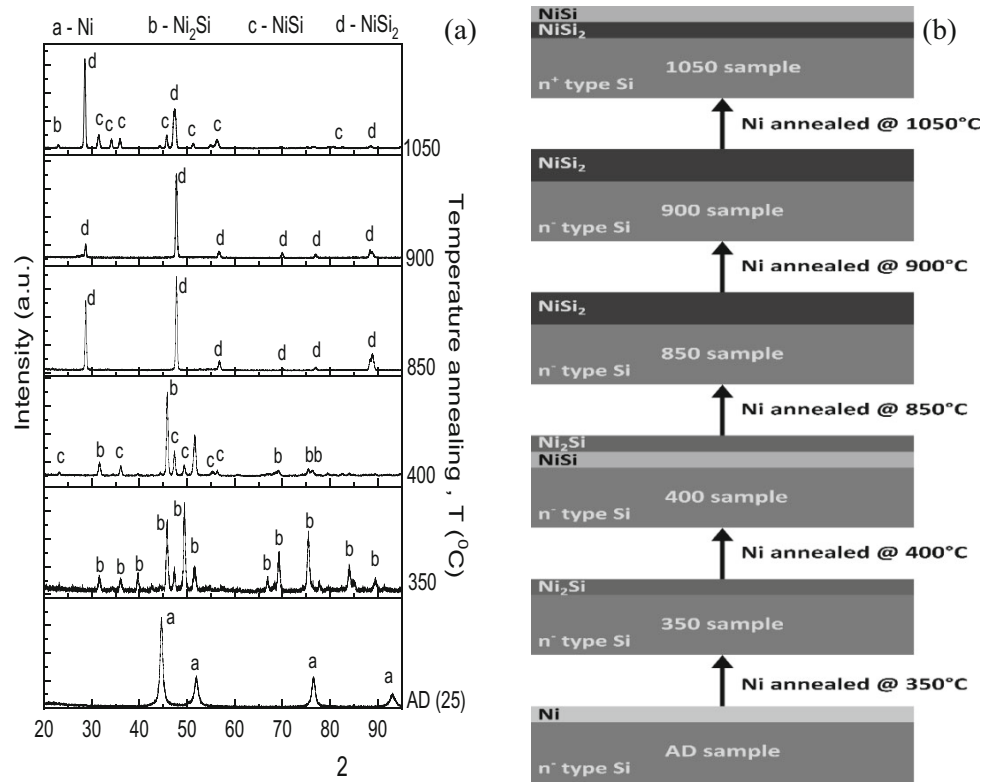
Grazing Incidence X-ray diffraction (GI-XRD) technique was employed to identify the constituent phases and to assess the microstructural parameters of the investigated samples using the SmartLab diffraction system (Rigaku Corporation, Tokyo, Japan) with CuK<sub>α1</sub> wavelength ( $\lambda = 1.5406 \text{ \AA}$ ). To acquire information from the thin films, the incidence angle was kept at a small value of 0.5° in all measurements, while the detector position was varied from 20 to 95°. The phase identification was performed by referring to the International Center for Diffraction Data (ICDD) database.

GI-XRD patterns recorded for both Schottky and ohmic MS contacts subjected to PMA treatments at different temperatures are shown Fig. 3a. It can be observed that the GI-XRD patterns are strongly dependent on the annealing temperature. According to the recorded patterns, the corresponding schematic cross-sectional view of the investigated structures illustrates the evolution of the nickel silicide interface layer as function of temperature annealing (Fig. 3b).

Thus, in the case of the as-deposited sample (*AD*), the diffraction peaks are located at 44.73°, 51.87°, 76.57°, 93.15° and they can be assigned unambiguously as Ni phases (card no. 001-1258) with lattice parameters  $a = b = c = 0.35 \text{ nm}$  that belong to Fm3m(225) space group. In contrast, the X-ray patterns corresponding to all the annealed samples (350–1050) show no traces of Ni or Si peaks, indicating that thermally activated interaction between Ni and Si occurs when the structures are subjected to PMA treatments, for the whole range of the investigated temperatures. Here, different Ni<sub>*x*</sub>Si<sub>*y*</sub> phases become visible. At low temperatures (350 and 400 °C), the orthorhombic Ni<sub>2</sub>Si phase with  $a = 0.73 \text{ nm}$ ,  $b = 0.99 \text{ nm}$  and  $c = 0.70 \text{ nm}$  (card no. 003-0943) is the dominant phase. At high temperatures (850 and 900 °C) the occurrence of cubic NiSi<sub>2</sub> phase (card no. 043-0989) with  $a = b = c = 0.53 \text{ nm}$  is evident, indicating an increased consumption of Si during the



**Fig. 3 a** GI-XRD patterns recorded for the as-deposited sample (AD) and PMA samples (350–1050), respectively. The peaks are indexed with letters corresponding to: a-Ni, b-Ni<sub>2</sub>Si, c-NiSi and d-NiSi<sub>2</sub>; **b** Schematic diagram of the nickel silicide (Ni<sub>x</sub>Si<sub>y</sub>) evolution as function of temperature of PMA treatments



annealing. Similar results were reported by Bahabry et al. [4], where the evolution of Ni<sub>x</sub>Si<sub>y</sub> stoichiometry with rapid thermal annealing processes from Ni<sub>2</sub>Si to NiSi, and further to NiSi<sub>2</sub> was showed. A different behaviour can be observed when the highest temperature annealing (1050 °C) is used for the ohmic contact, where a mixture of different phases was obtained. NiSi is the dominant phase (card no. 038-0844) with  $a = 0.52$  nm,  $b = 0.32$  nm and  $c = 0.56$  nm. Besides, the preferential orientation of NiSi<sub>2</sub> is modified from (220) to (111) in the presence of NiSi (see Fig. 4). The behaviour found at high temperatures appears different from the ones recently obtained on SiC substrate, where Ni<sub>2</sub>Si phase was identified for both 750 and 1050 °C [19]. It attests practically the central role played by substrate in the resulted Ni<sub>x</sub>Si<sub>y</sub> stoichiometry. Accordingly, the XRD analysis provides an indication of electrical performances to be expected, since the NiSi phase has the lowest reported electrical resistivity [25, 26] and it is the most appropriate candidate for the ohmic contact.

To gain further insights regarding the size of the crystalline domains and the lattice strain, we performed Rietveld refinement, which is based on the least squared method, where the experimental pattern is fitted with a theoretical line [27]. The strength

of this method lies in accounting all ( $hkl$ ) reflections, and thus the results enclose information brought by each of reflections. Figure 4 presented both the theoretical profile (red curve) and the experimental data (black curve) with different fitting parameters using least squares fitting.

As it can be observed, the theoretical profiles describe adequately the experimental ones, the small values of the fitting parameters indicating the goodness of the fit. The S parameter, called the scale factor, is close to unity for all samples, while the weighted parameter ( $R_{wp}$ ) varies from 17 to 32.5%. The last one indicates the relation between observed and calculated intensities of the measurement. The relative high  $R_{wp}$  values are determined by the background noise. Accordingly, the effective crystallite size ( $l$ ) and the root mean square strain ( $\langle \epsilon^2 \rangle^{1/2}$ ) of the resulted Ni and Ni<sub>x</sub>Si<sub>y</sub> phases have been determined (the values are listed in Table 1).

In addition to Debye–Scherrer method, using the Rietveld refinement, we were able to separate the effect of the crystallite size from the lattice strain one in the total peak broadening, which usually is not an easy task. Seibt et al. [28] showed that the bounding dislocations of a nickel silicide phase represents one

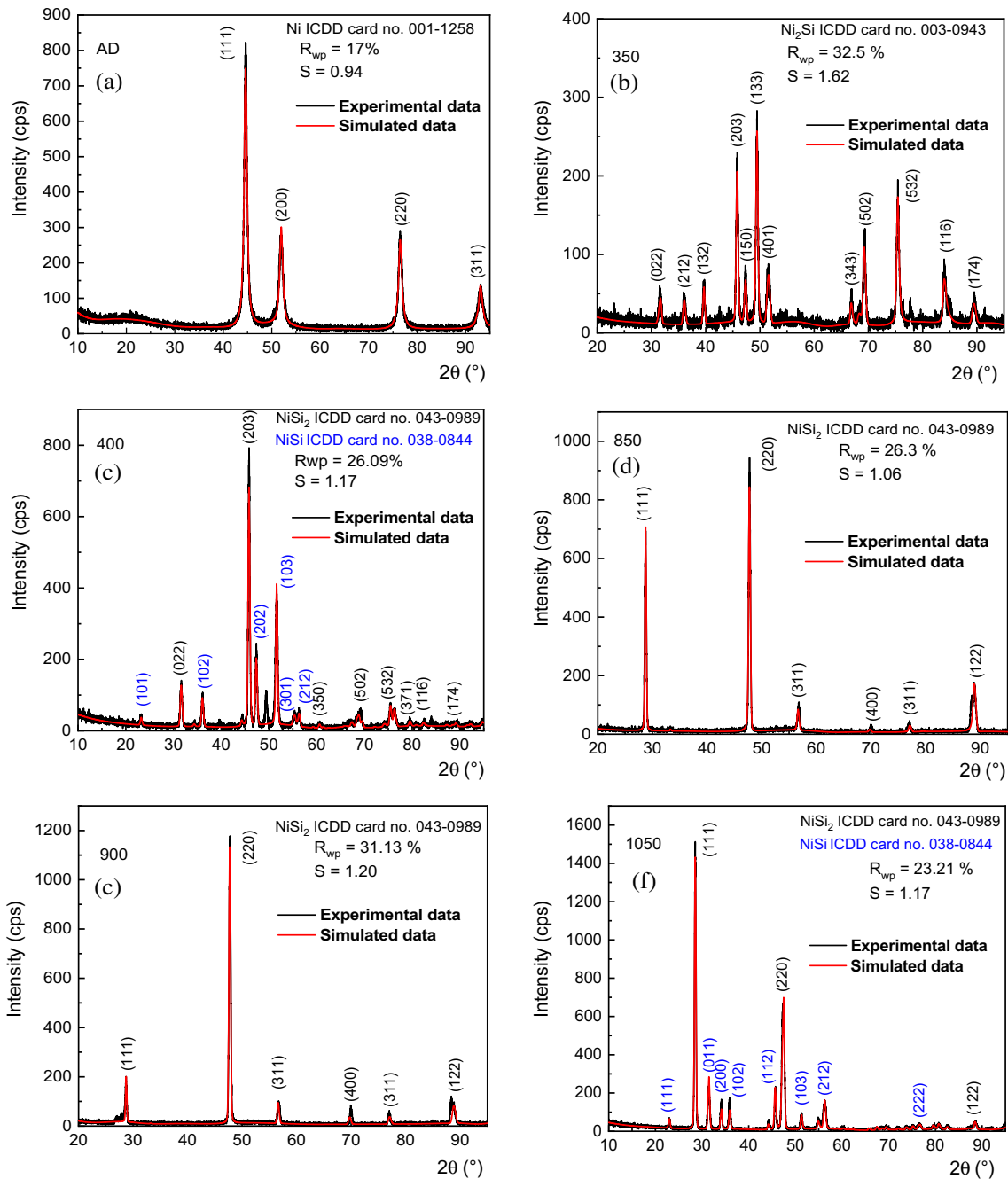


**Fig. 4** Experimental (black line) and the simulated curves (red curves) using Rietveld analysis for the as-deposited sample (AD) and PMA samples (350–1050), respectively. The fitting parameters

of the keys to understand the changes in electrical properties based on high-resolution transmission electron microscopy and deep level transient spectroscopy results. We used here the procedure developed by Williamson and Smallman [29] to determine the dislocation density ( $\rho_d$ ) corresponding to each of the fabricated samples with the formula:

$R_{wp}$  and  $S$  obtained using least square fitting method are listed as inset. The identification of diffraction peaks was achieved using ICDD database (Color figure online)

$$\rho_d = \frac{\sqrt{12} \langle \epsilon^2 \rangle^{1/2}}{l_{hkl}} \quad (1)$$

where  $d_{hkl}$  is the interplanar spacing on the preferential orientation, taken as the reflection which exhibit the highest intensity and calculated using the Bragg's law ( $2d \sin \theta = \lambda$ ,  $\lambda = 1.5406 \text{ \AA}$ ).

**Table 1** The mean crystallite size, the root mean square (rms) strain, the interplanar spacing and the dislocation density for the investigated samples

Sample	Mean crystallite size, $l$ (nm)	Root mean square strain, rms $\langle \varepsilon^2 \rangle^{1/2}$ (%)	Interplanar spacing, $d_{hkl}$ (nm)	Dislocation density $\times 10^{11}$ , $\rho_d$ (cm $^{-2}$ )
AD	9.97	0.27	0.203	4.62
350	16.8	0.23	0.184	2.57
400	20.2	0.19	0.197	1.65
850	29.7	0.15	0.190	0.92
900	37.7	0.12	0.190	0.58
1050	22.4	0.15	0.313	0.74

The following preferential orientations were observed in the X-ray patterns: Ni (111) located at  $2\theta = 44.62^\circ$  (*AD sample*), Ni<sub>2</sub>Si (002) at  $49.42^\circ$  (*350 sample*), Ni<sub>2</sub>Si (232) at  $45.79^\circ$  (*400 sample*), NiSi<sub>2</sub> (220) at  $47.71^\circ$  (*850 and 900 samples*) and NiSi<sub>2</sub> (111) at  $28.44^\circ$  (*1050 sample*). It can be noted that the dependence on the interplanar spacing indicates clearly that the dislocation density can be correlated with incorporation of the interstitial nickel atoms on the substitutional sites of the silicon lattice during formation of different phases of nickel silicide compounds [28]. The values calculated for microstructural parameters are summarised in Table 1.

Analysing the Schottky contacts' microstructural parameters, we can see that the crystallite size increases almost linearly up to 900 °C, where it reaches 37.7 nm, starting from 9.97 nm for the *AD* sample. On the other hand, the strain decreases with the temperature increasing, being around 0.12% at 900 °C. Consequently, we obtained a three-fold higher value for the crystallite size and, concomitant, a diminishing at more than twice the lattice strain when the temperature annealing increases up to 900 °C. Regarding the values obtained for the root mean square strain, they are comparable with the ones previously reported [30, 31], even lower in our case at low temperature annealing (300 and 400 °C).

Tung et al. [32] showed that codeposition of Ni<sub>2</sub>Si and a high temperature annealing (> 700 °C) reduce the dislocation density. Our results display a similar trend, the dislocation density decreasing with PMA temperature with almost one order of magnitude, from  $4.62 \times 10^{11}$  cm $^{-2}$  for *AD sample* to  $0.58 \times 10^{11}$  cm $^{-2}$  in the case of the *900 sample*. These values are more than one order of magnitude lower

in comparison with the ones previously reported in literature. For instance, Kolonits et al. reported values between  $9\text{--}176 \times 10^{12}$  cm $^{-2}$  for a Ni film electrodeposited using different aqueous electrolytes [33], with more than two orders of magnitude higher than our best performing sample (i.e. *900 sample*). Moreover, Csiszar et al. reported, on the one hand, almost one order of magnitude higher values ( $1.6 \times 10^{12}$  cm $^{-2}$ ) for a sample annealed at 400 °C and on the other hand, more than three orders of magnitude higher values ( $23 \times 10^{13}$  cm $^{-2}$ ) for the as-deposited one [34].

For the *1050 sample*, the ohmic contact with highly doped substrate, where a mixture of different phases was showed (NiSi and NiSi<sub>2</sub>), intermediary values for both mean crystallite size and dislocation density have been obtained. This different behaviour might be determined by the different properties of the Si substrate, which was firstly subjected to *P* diffusion process.

In order to establish the impact of the microstructural parameters on the device performances, the test structures were further electrically characterised using a Keithley 4200 semiconductor characterization system, at room temperature and dark conditions.

## 3.2 Electrical characterization of the resulted Ni/n-type contacts

### 3.2.1 Ohmic contacts

The Transfer Length Method implies measuring the resistance values between a series of pads with different spacing ( $d$ ), as it can be seen in Fig. 1. Representing the total resistance ( $R_T$ ) as a function of  $d$  and performing a linear fit, the intercept ( $a$ ) and the slope ( $b$ ) obtained are next used to determine the

main parameters of the ohmic contact based on the following formulas [35]:

$$R_T = 2R_c + \left(\frac{R_{sh}}{W}\right)d \quad (2)$$

$$a = 2R_c \rightarrow R_c = \frac{a}{2} \quad (3)$$

$$b = \frac{R_{sh}}{W} \rightarrow R_{sh} = b * W \quad (4)$$

$$\rho_c = \frac{W^2 R_c^2}{R_{sh}} \quad (5)$$

$$L_T = \sqrt{\frac{\rho_c}{R_{sh}}} \quad (6)$$

where:  $R_T$  is the total resistance obtained from a linear fit (reverse slope) on the I–V characteristics,  $R_c$  is the contact resistance,  $R_{sh}$  is the sheet resistance,  $W$  is the pads width,  $d$  is the distance between pads,  $a$  and  $b$  are the intercept and the slope obtained after the linear fit,  $\rho_c$  is the specific contact resistivity and  $L_T$  is the transfer length, which is practically the distance over which most of the current transfers from the semiconductor into the metal or from the metal into the semiconductor [36].

The obtained I–V characteristics for the two types of ohmic contacts employed are presented in Fig. 5: the control structure—as deposited Ni (*AD* sample—Fig. 5a) and the structure subjected to a PMA treatment at a temperature of 1050 °C (*1050* sample—Fig. 5b).

It can be observed that, whereas the electrical characteristics recorded for the *AD* sample present a deviation from linearity in the higher voltage domain, their aspect is significantly improved after the PMA treatment. Thus, a linear variation of the I–V characteristics on the entire range of the applied voltage was achieved. Next, using the I–V characteristics, the total resistance ( $R_T$ ) was calculated and plotted as function of the distance between pads in Fig. 6.

As it can be seen, the total resistance increases with distance and, more important, has almost twofold lower values after the PMA treatment. This diminishing of the total resistance is determined by the PMA treatment via formation of the nickel silicide compounds with improved electrical properties in comparison with Ni film. Using Eqs. (2)–(6), the electrical parameters of the ohmic contacts were calculated taking into account possible error expressions

reported in [35]. The obtained values are listed in Table 2.

We notice that the significant improvement of both microstructural and electrical parameters demonstrates undoubtedly the necessity of the high temperature PMA treatment. Thus, the sheet resistance, obtained using the Eq. (4), presents a higher value in the case of the annealed structures due to a more scattering of the film [37]. The contact resistance drops by half, indicating an easier way for current to pass through the metal/semiconductor interface. It is notable the low contact resistance achieved for the ohmic contact, favourable especially when it is used to bias the vertical type structures, as the vertical Schottky diode, where the contact resistance is in strong correlation with the device series resistance. As result, a low series resistance for the final device leads to less loss during the operation.

Next, we will analyse the specific contacts resistivity, which is the main electrical parameter of an ohmic contact that characterises not only the interfacial quality of the MS junction, but also the regions located both above and below the interface are cross-examined. This parameter is strongly influenced by another important factor in functionality of such contact, namely the transfer length, which provides information about the interface quality of the nickel silicide/Si system. Therefore, we have obtained a longer transfer length for the *AD* sample, making the current to flow longer distances under the contact to get through the metal. An illustration of this phenomenon is presented in Fig. 7.

Thus, for low transfer length (*1050* sample) the current flows quickly into the contact and only a little part of the contact edge is used in conduction. This case implies a lower specific contact resistivity with a value of  $3.6 \times 10^{-3} \Omega \text{ cm}^2$ . On the contrary, for higher values of  $L_T$  (*AD* sample), the current path is prolonged due to higher specific contact resistivity ( $2.4 \times 10^{-2} \Omega \text{ cm}^2$ ) and a larger portion of the contact is used for conduction. These high values for the specific contact resistivity could be attributed to an insufficient diffusion of the phosphorous on the Si backside. This fact can lead to a low donor doping density for such ohmic contacts. A detailed analysis regarding the dependence of the specific contact resistivity as a function of doping density is presented in [38], where we found that our phosphorous doped samples range between  $10^{18}$  and  $10^{19} \text{ cm}^{-3}$  in terms of donor density.



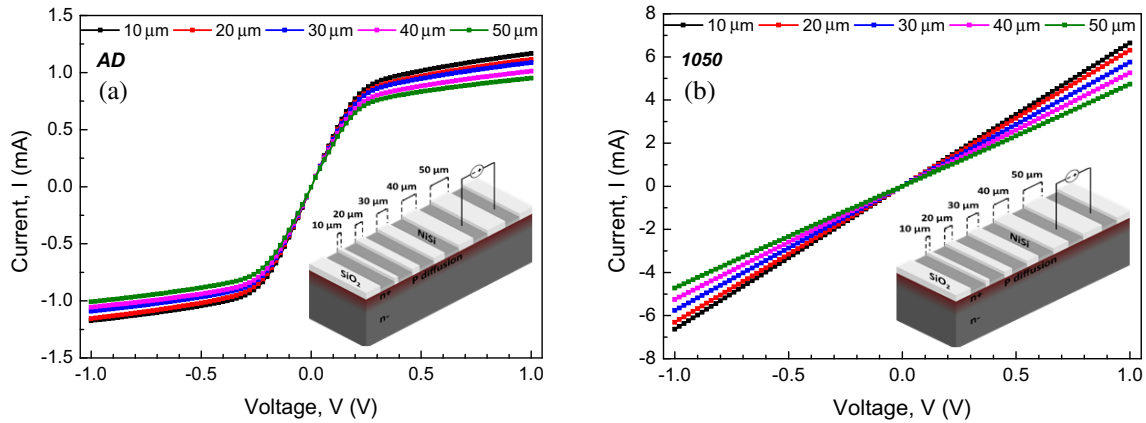


Fig. 5 I–V characteristics for the fabricated ohmic contacts: a AD sample; b 1050 sample

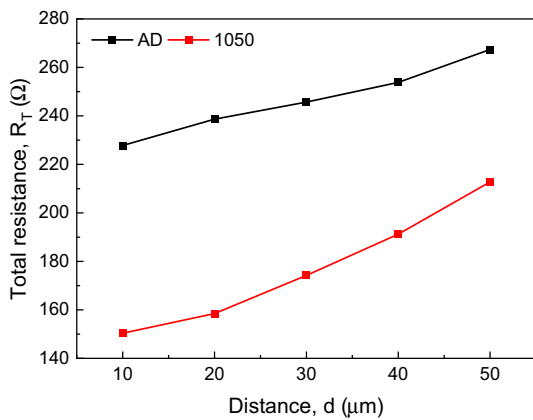


Fig. 6 The total resistance as function of the distance between pads for the two fabricated ohmic contacts

Table 2 The electrical parameters for the fabricated ohmic contacts

Sample	$R_{sh}$ ( $\Omega/\Upsilon$ )	$R_c$ ( $\Omega$ )	$L_T$ ( $\mu\text{m}$ )	$\rho_c$ ( $\Omega\text{cm}^2$ )
AD	113.5	111.6	147.5	$2.4 \times 10^{-2}$
1050	245.5	62.7	38.3	$3.6 \times 10^{-3}$

It should be mentioned that calculation of the transfer length aids an optimum contact design because, on the one hand, small contact lengths can generate current crowding and, on the other hand, a large contact length could represent a waste of usable device area.

### 3.2.2 Vertical Schottky diodes

Forward characteristics of Ni/Si Schottky rectifiers are presented in Fig. 8 and, as it can be observed, they follow thermionic emission theory [17].

At a first glance, we notice, as expected, the lowest level of the rectifying current displayed by the control sample (*AD sample*). Moving on to the annealed samples, they show an increase in current with the PMA temperature, reaching almost two orders of magnitude higher values for the *850* and *900 samples*. This behaviour can be attributed to the improvement of the crystal quality, which is further related to the lower dislocation density, according to XRD results, as well as a more homogenous nickel silicide/Si interface [23].

The main parameters for a Schottky diode (ideality factor— $n$ , Schottky barrier height— $SBH$ , saturation current— $I_s$  and series resistance— $R_s$ ) were extracted using the equation describing the thermionic emission conduction mechanism at the Schottky interface [17]:

$$I = A_n A_j T^2 \exp\left(-\frac{\Phi_{Bn}}{V_{th}}\right) \exp\left(\frac{V - IR_s}{nV_{th}}\right) \quad (7)$$

where  $A_n$  is the Richardson’s constant for electrons,  $A_j$  is the junction area,  $T$  is the temperature,  $\Phi_{Bn}$  is the Schottky barrier height (SBH),  $n$  is the ideality factor,  $R_s$  is the series resistance and  $V_{th} = kT/q$  is the thermal voltage, where  $k$  is the Boltzmann’s constant and  $q$  is the elementary charge.

The  $n$  and  $SBH$  plots as a function of annealing temperature are presented in Fig. 9a. As can be seen, while the  $n$  successively decreases,  $SBH$  increases with temperature. The higher values of  $n$  and

**Fig. 7** Current flow into the contact for the two types of the ohmic contacts

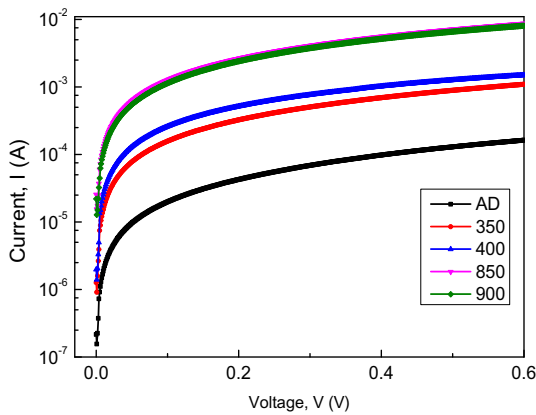
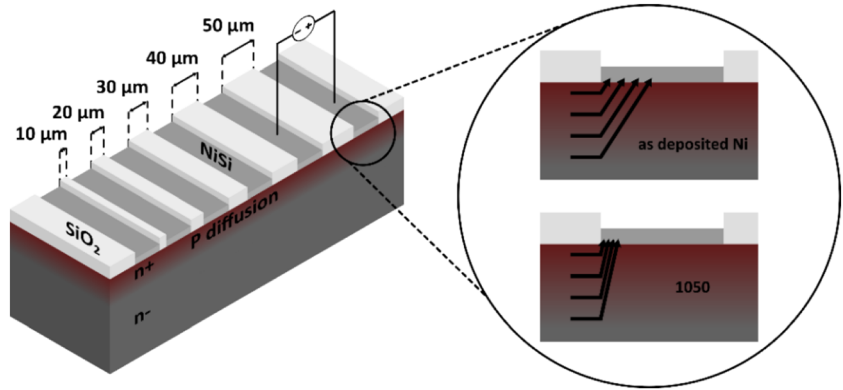


**Fig. 8** Forward I–V characteristics of the Schottky diodes, measured at room temperature

lower SBH obtained for AD and low temperature annealing samples might be determined by the inhomogeneities present at metal/semiconductor interface, defects revealed using electron microscopy techniques [24]. This behaviour confirms formation of a more homogenous Schottky contact during the high

temperature process. Therefore, if the Schottky contact contains many patches with low SBHs, where the current transport will be preferentially directed, the electrons are able to surmount these barriers (AD and low temperature annealing samples). As the annealing temperature is increasing, the Schottky contact presents less inhomogeneities at the metal/semiconductor interface and the dominant SBH will increase from 0.52 to 0.637 eV, the results being consistent with the ones previously reported in literature at room temperature [39, 40].

Also, it can be observed in Fig. 9b that the saturation currents and the series resistances are significantly improved when the PMA temperature increases. On the one hand, the saturation current decreases continuously with the annealing temperature, reaching a value of 0.246  $\mu\text{A}$  in the case of the sample annealed at 900  $^{\circ}\text{C}$ , which is nearly two orders of magnitude diminished in comparison with the control sample (AD sample). On the other hand, the series resistance starts from a value of 465.3  $\Omega$  in

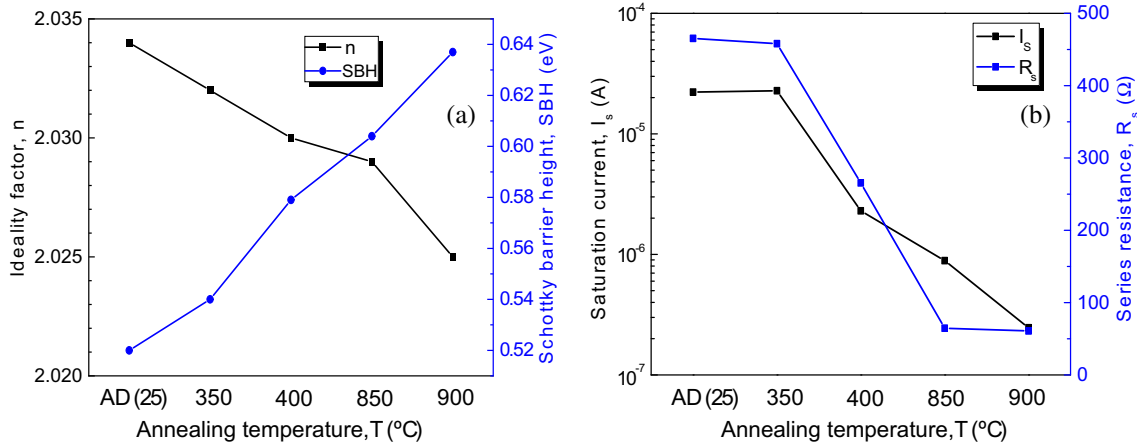


**Fig. 9** **a** The SBHs and the ideality factors; **b** the saturation currents and the series resistances of the fabricated vertical Schottky diodes

the case of the control sample and reaches a value almost eight times lower, around 60 Ω, when the sample was annealed at 900 °C.

### 3.2.3 Back-to-back Schottky diodes

Back-to-back Schottky diodes are devices with two identical Schottky areas defined on the semiconductor and are of great importance in applications that require photodetection [41]. In our case, the back-to-back Schottky contact configuration was used to obtain information about the rectifying current at different stages during the phase transition of the nickel silicide compounds. One of the benefits of the back-to-back Schottky configuration is that, in contrast with the standard vertical Schottky diode, the series resistance resulted from the semiconductor substrate can be neglected [42], bringing a substantial advantage in our estimations. Concerning their electrical behaviour, it is apparently an ohmic one due to the two back-to-back Schottky barriers formed even at low bias voltages. Consequently, when a voltage sweep is applied, one of the barriers is depleted and the electrical behaviour is similar with the one corresponding to the reverse bias mode.

The measured I–V characteristics are presented in Fig. 10a. As it can be seen, the current systematically increases with the PMA temperature, reducing significantly (almost one order of magnitude in current variation from AD to 900 sample) the Ni<sub>x</sub>Si<sub>x</sub> layer resistivity.

Similar behaviour was recently observed by Zhao et al. [43], where the current in a back-to-back Schottky diodes type structure was approximately double (at ± 1 V) after a process of CF<sub>4</sub> plasma immersion ion implantation (PIII) in Si. In comparison, our work reported a more significantly current

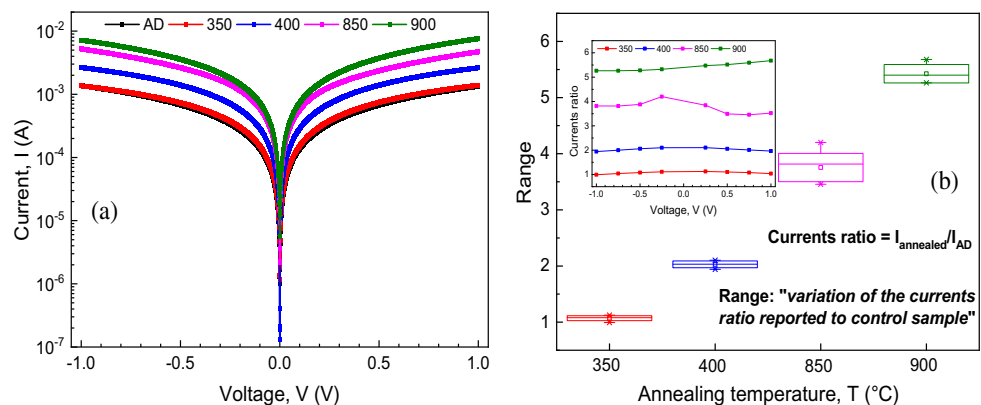
increase (almost six times) after the best performing post-metallization annealing process (900 °C).

In order to evaluate the range of the currents' variation, we have calculated the ratio between the currents obtained for the annealed samples ( $I_{\text{annealed}}$ ) and the ones obtained for the control sample ( $I_{\text{AD}}$ ) at different 8 fixed voltage (− 1, − 0.75, − 0.5, − 0.25, 0.25, 0.5, 0.75 and 1 V). The plots presented in Fig. 10b show a small range of variation for the samples annealed at low temperature (350 and 400 samples), with a twofold increase in current with temperature annealing ( $I_{400} > I_{350}$ ). Instead, in the case of the high temperature annealed samples (850 and 900 samples), we can observe a higher range of currents' variation and a more pronounced increase of the current, reaching a value of around six times higher in comparison with the control sample (AD sample). The currents' ratio for the annealed samples against the control one is plotted for each voltage in the inset graph.

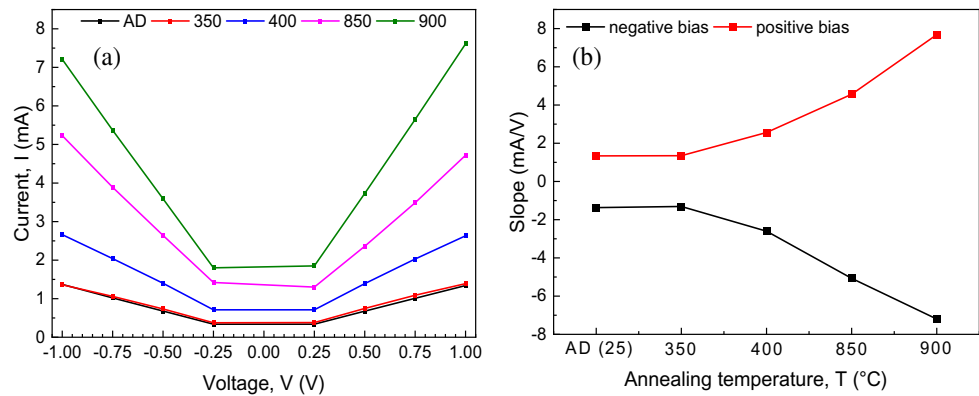
In addition, the variation of the currents at the above-mentioned fixed bias voltages was plotted in Fig. 11a. Next, we used a linear fit for the I–V characteristics on both positive and negative sides, to estimate the corresponding slopes for each of the fabricated sample and their corresponding values were plotted in Fig. 11b.

Figure 11a shows an improvement in both directions from around 1 mA for AD sample up to over 7 mA in the case of 900 sample at ± 1 V applied voltage. The current increase observed is determined by both the crystallinity improvement of the nickel silicide films and reduction of the dislocation density, according to the XRD analysis. In the same time, Fig. 11b shows an almost symmetrical variation of the slope values on the both positive and negative bias voltages. The slope variation increases with

**Fig. 10** a I–V characteristics of the fabricated back-to-back Schottky diodes and b corresponding current increasing at different fixed voltages



**Fig. 11** **a** Variation of the currents at different 8 fixed voltage and **b** slope variation of the current with applied voltage for each fabricated sample



temperature annealing, the highest value of  $\pm 8$  mA/V being obtained for the 900 sample.

## 4 Conclusions

Three types of metal/semiconductor structures have been designed and fabricated adjusting the Ni/n-type Si junction: (i) ohmic contacts annealed at very high temperature (1050 °C) in order to obtain a smooth metal/semiconductor interface and nickel silicide compounds with as low as possible specific contact resistivity; (ii) vertical Schottky diodes with the best performing ohmic contact on the backside wafer; (iii) back-to-back Schottky diodes with identical designed areas. The Schottky diodes were annealed at different temperatures up to 900 °C. The fabricated test structures were subjected to both microstructural investigations and electrical characterizations and the results were corroborated to reveal the connection between the microstructural parameters, such as phase changes, crystallite size and dislocation density, and the electrical performances and to indicate in what way they act. The structural improvements have been found in a more properly operation of the final devices, where a two times improvement for contact resistance in the case of the ohmic contact (1050 sample) have been reported. For both vertical and back-to-back Schottky diodes, an improving in rectifying performances with annealing temperature was obtained. For example, an increasing in current with almost two order of magnitude in the case of the vertical Schottky diodes and an almost six times current increasing (the case of the back-to-back Schottky diodes) were reported. All the results indicate the strong impact between the amounts of the dislocations emerged from the

boundaries of the adjacent crystallites and the electrical parameters. The proposed experimental study provides the necessary parameters to select the most appropriate technological process flow in order to fabricate very stable Ni/Si ohmic and Schottky contacts that present superior electrical performances.

## Acknowledgements

This work was supported by a grant of the Romanian Ministry of Education and Research, CNCS – UEFISCDI, project number PN-III-P1-1.1-PD-2019-0924, within PNCDI III. The authors thank P. Varasteanu for schematic views of the test structures.

## Declarations

**Conflict of interest** There are no conflicts to declare.

## References

1. R.T. Tung, Appl. Phys. Rev. **1**, 011304 (2014)
2. Y. Hu, J. Vac. Sci. Technol. A **16**, 1820 (1998)
3. D. Connétable, O. Thomas, J. Alloys Compd. **509**, 2639 (2011)
4. R.R. Bahabry, A.N. Hanna, A.T. Kutbee, A. Gumus, M.M. Hussain, Energy Technol. **6**, 1627 (2018)
5. Y. Yang, H. Xuan, X. Li, B. Zhang, X. Dong, S. Sun, Q. Cai, X. Xu, X. An, M. Li, Semicond. Sci. Technol. **35**, 035014 (2020)
6. A. Schrauwen, J. Demeulemeester, A. Kumar, W. Vander-vorst, C.M. Comrie, C. Detavernier, K. Temst, A. Vantomme, J. Appl. Phys. **114**, 063518 (2013)
7. M.C. Cheynet, R. Pantel, Micron **37**, 377 (2006)

8. N. Kawasaki, N. Sugiyama, Y. Otsuka, H. Hashimoto, M. Tsujimoto, H. Kurata, S. Isoda, *Ultramicroscopy* **108**, 399 (2008)
9. N. Kawasaki, N. Sugiyama, Y. Otsuka, H. Hashimoto, H. Kurata, S. Isoda, *J. Appl. Phys.* **109**, 063716 (2011)
10. E. Verleysen, H. Bender, O. Richard, D. Schryvers, W. Vandervorst, *J. Mater. Sci.* **46**, 2001 (2011)
11. R.J. Hauenstein, T.E. Schlesinger, T.C. McGill, B.D. Hunt, L.J. Schowalter, *Appl. Phys. Lett.* **47**, 853 (1985)
12. Q.T. Zhao, U. Breuer, E. Rije, S. Lenk, S. Mantl, *Appl. Phys. Lett.* **86**, 1 (2005)
13. Y.-J. Chang, J.L. Erskine, *Phys. Rev. B* **28**, 5766 (1983)
14. M. Sağlam, F.E. Cimilli, A. Türüt, *Phys. B* **348**, 397 (2004)
15. C. Detavernier, R.L. Van Meirhaeghe, R. Donaton, K. Maex, F. Cardon, *J. Appl. Phys.* **84**, 3226 (1998)
16. S. Zhu, R.L. Van Meirhaeghe, C. Detavernier, F. Cardon, G.-P. Ru, X.-P. Qu, B.-Z. Li, *Solid. State. Electron.* **44**, 663 (2000)
17. R.T. Tung, *Phys. Rev. B* **45**, 13509 (1992)
18. F. Draghici, G. Brezeanu, G. Pristavu, R. Pascu, M. Badila, A. Pribeanu, E. Ceuca, *Sensors* **19**, 2384 (2019)
19. R. Pascu, G. Pristavu, G. Brezeanu, F. Draghici, P. Godignon, C. Romanitan, M. Serbanescu, A. Tulbure, *Sensors* **21**, 942 (2021)
20. C.K. Kim, J.H. Lee, S.M. Choi, I.H. Noh, H.R. Kim, N.I. Cho, C. Hong, G.E. Jang, *Sens. Actuators B* **77**, 455 (2001)
21. R. Pascu, F. Craciunoiu, M. Kusko, F. Draghici, A. Dinescu, M. Danila, in *Proceedings of the International Semiconductor Conference CAS 2*, 457 (2012)
22. R. Pascu, F. Craciunoiu, M. Kusko, in *2013 9th Conference Ph.D. Research Microelectronics and Electronics (PRIME)*, (Villach, Austria, 2013), pp. 297–300
23. R. Pascu, C. Romanitan, O. Tutunaru, F. Comanescu, in *2019 International Semiconductor Conference* (2019), pp. 319–322
24. R. Pascu, M. Danila, P. Varasteanu, M. Kusko, G. Pristavu, G. Brezeanu, F. Draghici, in *Proceedings of the International Semiconductor Conference CAS* (2018), pp. 307–310.
25. B. Cafra, A. Alberti, L. Ottaviano, C. Bongiorno, G. Mannino, T. Kammler, T. Feudel, *Mater. Sci. Eng. B* **114–115**, 228 (2004)
26. T. Morimoto, T. Ohguro, H.S. Momose, T. Iinuma, I. Kunishima, K. Suguro, I. Katakabe, H. Nakajima, M. Tsuchiaki, M. Ono, Y. Katsumata, H. Iwai, *IEEE Trans. Electron Devices* **42**, 915 (1995)
27. H.M. Rietveld, *J. Appl. Crystallogr.* **2**, 65 (1969)
28. M. Seibt, H. Hedemann, A.A. Istratov, F. Riedel, A. Sattler, W. Schröter, *Phys. Status Solidi Appl. Res.* **171**, 301 (1999)
29. G.K. Williamson, R.E. Smallman, *Philos. Mag.* **1**, 34 (1956)
30. M.K. Datta, S.K. Pabi, B.S. Murty, *Mater. Sci. Eng. A* **284**, 219 (2000)
31. W.W. Wu, K.C. Lu, K.N. Chen, P.H. Yeh, C.W. Wang, Y.C. Lin, Y. Huang, *Appl. Phys. Lett.* **97**, 18 (2010)
32. R.T. Tung, A.F.J. Levi, J.P. Sullivan, F. Schrey, *Phys. Rev. Lett.* **66**, 72 (1991)
33. T. Kolonits, P. Jenei, B.G. Tóth, Z. Czigány, J. Gubicza, L. Péter, I. Bakonyi, *J. Electrochem. Soc.* **163**, D107 (2016)
34. G. Csiszár, K. Pantleon, H. Alimadadi, G. Ribárik, T. Ungár, *J. Appl. Crystallogr.* **45**, 61 (2012)
35. H.J. Ueng, D.B. Janes, K.J. Webb, *IEEE Trans. Electron Devices* **48**, 758 (2001)
36. D.K. Schroder, *Material and Device Semiconductor Material and Device*, 3rd edn. (Wiley, Arizona State University, New York, Tempe, 2006).
37. C.-T. Wu, Y.-J. Lee, F.-K. Hsueh, P.-J. Sung, T.-C. Cho, M.I. Current, T.-S. Chao, *ECS J. Solid State Sci. Technol.* **3**, 122 (2014)
38. J. Kim, P.J. Oldiges, H.F. Li, H. Niimi, M. Raymond, P. Zeitzoff, V. Kamineneni, P. Adusumilli, C. Niu, F. Chafik, in *International Conference on Simulation of Semiconductor Processes and Devices, SISPAD* (2015), pp. 234–237
39. S. Zhu, R.L. Van Meirhaeghe, S. Forment, G. Ru, B. Li, *Solid State Electron.* **48**, 29 (2004)
40. R. Kumar, S. Chand, *Solid State Sci.* **58**, 115 (2016)
41. M. Ahmetoglu, S.K. Akay, *Curr. Appl. Phys.* **10**, 652 (2010)
42. S. Zheng, Q.-Q. Sun, W. Yang, P. Zhou, H.-L. Lu, D.W. Zhang, *Nanoscale Res. Lett.* **8**, 116 (2013)
43. L.T. Zhao, M. Liu, Q.H. Ren, C.H. Liu, Q. Liu, L.L. Chen, Y. Spiegel, F. Torregrosa, W. Yu, Q.T. Zhao, *Nanotechnology* **31**, 205201 (2020)

**Publisher's Note** Springer Nature remains neutral with regard to jurisdictional claims in published maps and institutional affiliations.